

COMPRESSION AND RADIATION OF HIGH-POWER SHORT RF PULSES. I. ENERGY ACCUMULATION IN DIRECT-FLOW WAVEGUIDE COMPRESSORS

K. Sirenko

King Abdullah University of Science and Technology (KAUST)
4700 KAUST, Thuwal, 23955-6900, Saudi Arabia

V. Pazynin and Y. Sirenko

Institute of Radiophysics and Electronics
National Academy of Sciences of Ukraine (IRE NASU)
12 Acad. Proskura Str., Kharkiv, 61085, Ukraine

H. Bağcı

King Abdullah University of Science and Technology (KAUST)
4700 KAUST, Thuwal, 23955-6900, Saudi Arabia

Abstract—Proper design of efficient microwave energy compressors requires precise understanding of the physics pertinent to energy accumulation and exhaust processes in resonant waveguide cavities. In this paper, practically for the first time these highly non-monotonic transient processes are studied in detail using a rigorous time-domain approach. Additionally, influence of the geometrical design and excitation parameters on the compressor's performance is quantified in detail.

1. INTRODUCTION

A microwave (energy) compressor is a device capable of converting a long-duration low-amplitude input pulse into a short-duration high-amplitude output pulse. Active compressors achieve this by accumulating the energy of input pulse for a relatively long period of time and then exhausting the accumulated energy in the form of a short high-power output. Efficient microwave pulse compression is

needed in several fields of science and engineering: Compressors are used as components of particle accelerators [1, 2] and radars [3], and utilized in data transmission [4], energy transfer [5], plasma heating [6], and biological studies [7].

An active microwave compressor consists of a storage unit, which acts as an energy accumulator, and a switch, which terminates the energy accumulation in the storage unit and lets the accumulated energy exhaust [8]. Although the storage unit might be designed in a number of ways, the most common designs utilize high- Q waveguide cavities [1, 2, 9–14]. As for switches, a few design options exist: switches that change the resonance condition of the whole device via discharge [9, 14] or controlled effects in semiconductors [12, 15], distributed-grating type switches [16], interference plasma (gas discharge) switches [10, 13], trigatron commutators [11, 14], and resonant switches [17, 18]. Apparently, a compressor is a resonant device; its design and analysis require a detailed study of long-duration accumulation and short-duration exhaust processes involving weakly-decaying fields of quasi-monochromatic pulses. For proper operation of the compressor, the design parameters of the storage unit and the switch, and the input pulse parameters should be correctly fitted and completely consistent. A miscalculated variation in any of these parameters usually causes an avalanche of changes, which can dramatically reduce the compressor's performance. Unfortunately, the effect of these variations cannot be predicted using simplified and approximate mathematical models, which separately account for characteristics of compressor's isolated components. For example, design and characterization methods, which employ approximate mathematical models [1, 8, 9, 12] and experimental testing procedures [2, 14], do not take into account the time-dependent features of the compressors. Moreover, they require tuning of the compressors' design parameters manually [1, 2, 12, 14]. To this end, mathematically rigorous and accurate full-wave simulators, which model the compressor as a whole and throughout the entire duration of time-dependent energy accumulation and exhaust, should be utilized in design and analysis of compressors.

Time-domain methods are best suited for this job mostly because they allow real-time observation of all wave interactions taking place during the energy accumulation and exhaust. However, very long observation times required to study the transient resonant processes enforce two main constraints on the time-domain method used: (i) High accuracy to avoid error build up during long simulation times and to obtain reliable results; (ii) high efficiency to complete the simulations using reasonable computational resources. In this

work, finite-difference time-domain (FDTD) method described in [19] is preferred for this purpose. This simulator achieves high accuracy by employing mathematically exact absorbing boundary conditions (EACs) [19–21]. Its efficiency is increased via the use of a numerically exact blocked-FFT based scheme, which reduces the computational cost of temporal convolutions present in the non-local EACs [19, 22–28]. Combination of these two advanced computational techniques renders this FDTD simulator an ideal candidate for accurately analyzing the energy accumulation and exhaust in compressors.

It is not possible to design a properly functioning energy compressor without in-depth understanding of the energy accumulation process. The energy accumulation process, which involves formation of highly resonant high-power pulses in the storage unit, is non-uniform in time; hence, a real-time study is required to fully understand all pertinent physical phenomena. In this work, practically for the first time, all processes inside a compressor are studied in time-domain in detail from the very beginning of the excitation right until the end of the accumulated energy's exhaust. Moreover, the influence of various parameters of the compressor and the excitation on the energy accumulation process and, thus, the overall compressor's performance, is discussed. As an example, the paper analyzes in detail the energy accumulation processes in a rectangular direct-flow waveguide compressor excited by $TE_{0,n}$ waves, which is designed following the scheme outlined in [17]. This paper supplements [17]; together they allow for rigorously formulating and efficiently solving the problem of designing and analyzing various compressors in VHF, UHF, SHF and EHF bands (from 300 MHz to 300 GHz).

The novel contributions of this work are twofold: (i) It presents a rigorous scheme to design and characterize energy compressors, which allows to study a compressor as a whole in contrast to the existing design frameworks, which separately account for characteristics of the compressor's isolated components. The proposed method is capable of performing a fully rigorous characterization of the time-dependent energy accumulation and exhaust processes. (ii) A detailed discussion on the effects of the various design parameters (geometric dimension, switching, etc.) and the durations of the excitation and energy accumulation and exhaust processes on the efficiency of the compressor is presented.

The remainder of this paper is organized as follows. Section 2 starts with a description of the mathematical model, and then introduces several time- and frequency-domain characteristics used in the design and analysis of the compressors. Section 3 starts with a brief summary of the design scheme used, and then presents a detailed

discussion of the energy accumulation processes and explains how various parameters of the compressors and the excitation influence the compressor's performance. Section 4 provides a short description of the FDTD simulator with FFT-accelerated EACs. Section 5 presents conclusions and future research avenues.

2. MATHEMATICAL MODEL AND CHARACTERISTICS OF MICROWAVE COMPRESSORS

This section first introduces the mathematical model (Section 2.1), and then describes the compressor's time- and frequency-domain characteristics in terms of model parameters (Sections 2.2 and 2.3). It should be noted here that the mathematical model parameters and the time and frequency domain characteristics are extensively referred to in Section 3, where the energy accumulation process is discussed in detail.

2.1. Mathematical Model

Consider the two-dimensional (2-D) model of the rectangular direct-flow waveguide compressor presented in Fig. 1. $TE_{0,n}$ wave interactions on this structure are mathematically modelled by the following initial-boundary value problem [20, 21]:

$$\begin{aligned} [-\varepsilon_r(g) \partial_t^2 - P + \partial_z^2 + \partial_y^2] U(g, t) &= 0; \quad t > 0, \quad g = \{y, z\} \in \mathbf{Q} \\ U(g, 0) &= 0, \quad \partial_t U(g, t)|_{t=0} = 0; \quad g \in \overline{\mathbf{Q}}_L \\ E_{tg}(g, t)|_{g \in \mathbf{S}} &= 0; \quad t \geq 0 \end{aligned} \quad (1)$$

Here, $\{x, y, z\}$ are Cartesian coordinates; $P[U] = \partial_t[Z_0\sigma_0(g, t)U(g, t)]$; $U = E_x$, $E_y = E_z = H_x = 0$; $\vec{E}(g, t) = \{E_x, E_y, E_z\}$ and $\vec{H}(g, t) = \{H_x, H_y, H_z\}$ are the vectors of electric and magnetic fields; \mathbf{S} represents the perfect electrically conducting (PEC) surfaces of the compressor; $E_{tg}(g, t)$ is the component of electric field that is tangential to \mathbf{S} ; $\mathbf{Q} = \mathbf{Q}_L \cup \mathbf{I} \cup \mathbf{II} \cup \mathbf{L}_1 \cup \mathbf{L}_2$ is the physical domain; $\mathbf{Q}_L = \{g = \{y, z\} \in \mathbf{Q} : -L_1 < z < L_2\}$ is the computation domain; $\sigma_0(g, t)$ and $\varepsilon_r(g)$ represent the conductivity and the relative permittivity; $Z_0 = (\mu_0/\varepsilon_0)^{1/2}$, ε_0 and μ_0 are the wave impedance, permittivity and permeability of the free space, respectively. $\sigma_0(g, t)$ and $\varepsilon_r(g)$ are piecewise constant functions in space, and the conductivity's time dependence is utilized to change the compressor's mode of operation (energy accumulation/exhaust). Domains $\mathbf{I} = \{g \in \mathbf{Q} : -a_1/2 \leq y \leq a_1/2, z < -L_1\}$,

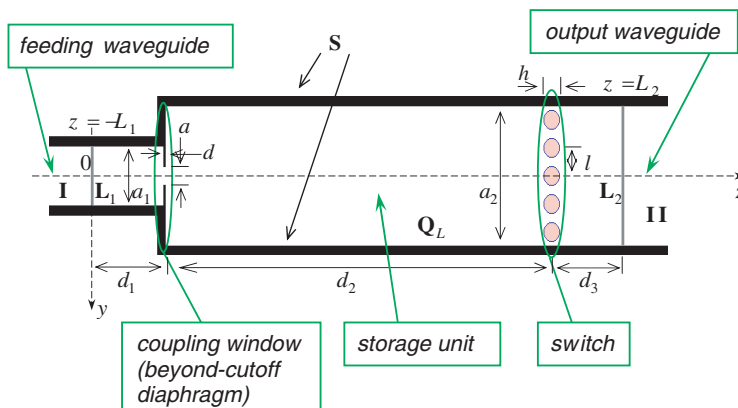


Figure 1. Geometry of a direct-flow compressor on the basis of rectangular waveguides.

and $\mathbf{II} = \{g \in \mathbf{Q} : -a_2/2 \leq y \leq a_2/2, z > L_2\}$ represent infinite regular input (feeding) and output waveguides, and contours $\mathbf{L}_1 = \{g \in \mathbf{Q} : z = -L_1\}$ and $\mathbf{L}_2 = \{g \in \mathbf{Q} : z = L_2\}$ represent virtual boundaries between \mathbf{I} and \mathbf{II} and the computation domain \mathbf{Q}_L , respectively. The physical domain \mathbf{Q} is unbounded in the z (longitudinal) direction. In this model, the SI system is used for all physical quantities except the time t , which is multiplied with the speed of light in free space and measured in meters.

Let $U^i(g, t)$ represent an incident pulse (excitation), which arrives from the feeding waveguide \mathbf{I} upon the virtual boundary \mathbf{L}_1 at time $t > 0$. The total field $U(g, t)$ in \mathbf{I} can be represented as a sum of incident and scattered fields: $U(g, t) = U^i(g, t) + U_1^s(g, t)$, $g \in \mathbf{I}$; in \mathbf{II} total field consists of only the scattered field: $U(g, t) = U_2^s(g, t)$, $g \in \mathbf{II}$. $U^i(g, t)$, $U_1^s(g, t)$, and $U_2^s(g, t)$ are represented in terms of modes via separation of variables [20, 21]:

$$\begin{aligned}
 U^i(g, t) &= \sum_n v_{n,1}(z, t) \mu_{n,1}(y); \quad g \in \mathbf{I}, \\
 U_j^s(g, t) &= \sum_n u_{n,j}(z, t) \mu_{n,j}(y); \quad g \in \mathbf{I} \text{ for } j = 1, \\
 &g \in \mathbf{II} \text{ for } j = 2, \quad j = 1, 2.
 \end{aligned}
 \tag{2}$$

The spatio-temporal (mode) amplitudes $v_{n,1}(z, t)$ and $u_{n,j}(z, t)$ and

the transverse functions $\mu_{n,j}(y)$ are related by

$$\left\{ \begin{matrix} v_{n,1}(z,t) \\ u_{n,j}(z,t) \end{matrix} \right\} = \int_{-a_j/2}^{a_j/2} \left\{ \begin{matrix} U^i(g,t) \\ U_j^s(g,t) \end{matrix} \right\} \mu_{n,j}(y) dy; \quad g \in \mathbf{I} \text{ for } j = 1,$$

$$g \in \mathbf{II} \text{ for } j = 2, \quad j = 1, 2.$$

where a_j represent the widths of the waveguides \mathbf{I} ($j = 1$) and \mathbf{II} ($j = 2$) (Fig. 1). It should be noted that $v_{n,1}(z,t)$, $u_{n,j}(z,t)$ and $\mu_{n,j}(y)$ define a complete set of modes for representing the waves $U^i(g,t)$ and $U_j^s(g,t)$. The transverse functions $\mu_{n,j}(y)$ and the corresponding eigenvalues $\lambda_{n,j}$ are known; for the $TE_{0,n}$ waves in 2-D waveguides considered here, they are given by [20, 21]:

$$\mu_{n,j}(y) = \sqrt{\frac{2}{a_j}} \sin\left(n\pi \frac{y+a_j/2}{a_j}\right), \quad \lambda_{n,j} = \frac{n\pi}{a_j}; \quad n = 1, 2, 3, \dots, \quad j = 1, 2.$$

The unbounded (open) problem (1) in the domain \mathbf{Q} can be converted into a bounded (closed) one in the domain \mathbf{Q}_L , which is more suitable for numerical solution, by introducing EACs on the virtual boundaries \mathbf{L}_1 and \mathbf{L}_2 (Fig. 1). In this work, the EACs derived in [20, 21] are used. It should be noted here that enforcing EACs on virtual boundaries results in mathematically exact conversion of the unbounded problem to the bounded one [20, 21]. The EACs on \mathbf{L}_1 and \mathbf{L}_2 are [20, 21]:

$$U(y, -L_1, t) - U^i(y, -L_1, t) = \sum_n \left\{ \int_0^t J_0(\lambda_{n,1}(t-\tau)) \right.$$

$$\times \left. \left[\int_{-a_1/2}^{a_1/2} \partial_z [U(\tilde{y}, z, \tau) - U^i(\tilde{y}, z, \tau)]|_{z=-L_1} \mu_{n,1}(\tilde{y}) d\tilde{y} \right] d\tau \right\} \mu_{n,1}(y);$$

$$\frac{-a_1}{2} \leq y \leq \frac{a_1}{2}, \quad t \geq 0,$$

$$U(y, L_2, t) = - \sum_n \left\{ \int_0^t J_0(\lambda_{n,2}(t-\tau)) \right.$$

$$\times \left. \left[\int_{-a_2/2}^{a_2/2} \partial_z U(\tilde{y}, z, \tau)|_{z=L_2} \mu_{n,2}(\tilde{y}) d\tilde{y} \right] d\tau \right\} \mu_{n,2}(y); \quad \frac{-a_2}{2} \leq y \leq \frac{a_2}{2}, \quad t \geq 0.$$

Here, $J_0(\cdot)$ represents the Bessel function of the zeroth order. It should be noted here that these EACs are nonlocal both in space and time (note the ranges of integrals over τ and \tilde{y}); their direct numerical implementation results in increased computational requirements. This can be alleviated by using localization techniques [20,21] or by accelerating the computation of temporal convolutions via the use of blocked FFTs [22–28] as described in [19]. It should be noted here that both of these techniques are exact, i.e., their application does not introduce additional errors into the numerical solution.

2.2. Time-domain Characteristics

Four different characteristics are defined in the time-domain to quantify the energy accumulation and exhaust processes on compressors:

- (i) *Energy Efficiency* is the ratio of the useful output energy to the total input energy:

$$\eta = \frac{W_2^s(t_3; t_4)}{W_1^i(t_1; t_2)}. \tag{3}$$

Here, $W_1^i(t_1; t_2)$ and $W_2^s(t_3; t_4)$ represent the total energies fed into compressor from the waveguide **I** between times t_1 and t_2 , and transmitted into the output waveguide **II** between times t_3 and t_4 , respectively; t_1 and t_2 are the turn-on and off times of the excitation (t_1 is usually zero), the useful output pulse is non-zero between t_3 and t_4 . $W_1^i(t_1; t_2)$ and $W_2^s(t_3; t_4)$ are computed using:

$$W_j^{i(s)}(t_1; t_2) = - (+) \int_{t_1}^{t_2} P_j^{i(s)}(t) dt; \quad j = 1, 2, \tag{4}$$

where $-P_1^i(t)$ and $P_2^s(t)$ represent the instantaneous power entering and leaving the computation domain \mathbf{Q}_L through the virtual boundaries \mathbf{L}_1 and \mathbf{L}_2 , respectively and are computed by [32]:

$$P_j^{i(s)}(t) = \int_{\mathbf{L}_j} \left(\left[\vec{E}_j^{i(s)}(g, t) \times \vec{H}_j^{i(s)}(g, t) \right] \cdot \vec{n}_j \right) dS$$

$$= \begin{cases} - \int_{-a_1/2}^{a_1/2} \left[E_x^{i(s)}(y, -L_1, t) H_y^{i(s)}(y, -L_1, t) \right] dy & \text{for } j=1, g \in \mathbf{L}_1 \\ \int_{-a_2/2}^{a_2/2} \left[E_x^s(y, L_2, t) H_y^s(y, L_2, t) \right] dy & \text{for } j=2, g \in \mathbf{L}_2 \end{cases} \tag{5}$$

where \vec{n}_j represents the unit normal defined on the boundary \mathbf{L}_j which points outwards from the domain \mathbf{Q}_L , and $\vec{E}_j^{i(s)}(g, t)$ and

$\vec{H}_j^{i(s)}(g, t)$, $g \in \mathbf{L}_j$, are the boundary values of incident (scattered) electric and magnetic fields.

η is a positive number less than or equal to one, — obviously, the closer η to one, the more efficient compressor is.

- (ii) *Degree of Compression* quantifies how short the useful output pulse is in comparison to the input pulse — it is defined as the ratio of input and output pulse durations:

$$\beta = \frac{T^i}{T_2^s}, \quad (6)$$

where $T^i = t_2 - t_1$ and $T_2^s = t_4 - t_3$ are the durations of input and output pulses, respectively. Normally, β is a positive number greater than one – obviously, larger β means higher compression rate.

- (iii) *Power Gain* is a measure of compressor's ability to increase the power of the output pulse in comparison to the input pulse. Power gain is defined as the product of the degree of compression (6) and the energy efficiency (3):

$$\theta = \beta \cdot \eta \quad (7)$$

It is clear from (7) that θ is the ratio of the mean powers of the input and output pulses. θ is a positive number greater than one — obviously, larger θ means higher power gain.

- (iv) *Instantaneous Energy Accumulation Efficiency* is the ratio of the energy accumulated in the storage unit to the total input energy within a given length of time. The instantaneous energy accumulation efficiency at a given moment of time t is defined as

$$\eta_{accum}(t) = \frac{W_1^i(0; t) - W_1^s(0; t) - W_2^s(0; t)}{W_1^i(0; t)}, \quad (8)$$

where $W_1^s(t_1; t_2)$ represents the energy reflected back into the feeding waveguide \mathbf{I} between the times t_1 and t_2 (see (4)); meanings of $W_1^i(0; t)$ and $W_2^s(0; t)$ are already discussed above. According to the law of energy conservation (see below), in the absence of loss (i.e., under the assumption of PEC walls) the difference between the total input energy $W_1^i(0; t)$ and the reflected and transmitted energies $W_j^s(0; t)$, $j = 1, 2$ is equal to the energy accumulated in the storage unit.

$\eta_{accum}(t)$ is used in determining the optimal length of excitation T^i — the reflected and transmitted instantaneous powers are non-monotonic functions of time, which means that there are time intervals when the accumulated energy grows faster than the

scattered one, hence, $\eta_{accum}(t)$ also changes non-monotonically with time. For example, T^i can be set to maximize the overall energy efficiency η ; this can be achieved by turning off the excitation at the time when $\eta_{accum}(t)$ is maximum. One may trade maximum η for the highest possible energy in the output pulse, and, accordingly, the highest power gain; this can be achieved by turning off the excitation when the accumulated energy is not growing any more – the storage cannot accept energy any more.

The understanding of the above characteristics is completed by adding a short discussion on the balance of instantaneous power (the instantaneous Poynting theorem), which reads [32]

$$\underbrace{P_1^s(t) + P_1^{i \times s}(t) + P_2^s(t)}_1 + \underbrace{\frac{1}{2} \frac{\partial}{\partial t} \int_{\mathbf{Q}_L} (Z_0 |\vec{H}(g, t)|^2 + \frac{\epsilon_r(g)}{Z_0} |\vec{E}(g, t)|^2) dV}_2 + \underbrace{\int_{\mathbf{Q}_L} \sigma_0(g) |\vec{E}(g, t)|^2 dV}_3 = -P_1^i(t). \tag{9}$$

Here, $\vec{E}(g, t)$ and $\vec{H}(g, t)$ are electric and magnetic fields, $dV = dydz$, $P_j^s(t)$, $j = 1, 2$ and $P_1^i(t)$ are given by (5), and the $P_1^{i \times s}(t)$ is given by

$$\begin{aligned} P_1^{i \times s}(t) &= \int_{\mathbf{L}_1} \left[\left([\vec{E}_1^s \times \vec{H}_1^i] + [\vec{E}_1^i \times \vec{H}_1^s] \right) \cdot \vec{n}_1 \right] dS \\ &= - \int_{-a_1/2}^{a_1/2} \left[E_x^s(y, -L_1, t) H_y^i(y, -L_1, t) \right. \\ &\quad \left. + E_x^i(y, -L_1, t) H_y^s(y, -L_1, t) \right] dy. \end{aligned}$$

Indeed, as it is clearly stated by (9) that the sum of the instantaneous power reflected and transmitted from the domain \mathbf{Q}_L into the waveguides **I** and **II** through the boundaries \mathbf{L}_1 and \mathbf{L}_2 (term 1), the instantaneous power accumulated in \mathbf{Q}_L (term 2), and the instantaneous power dissipated due to loss in \mathbf{Q}_L (term 3) is equal to the instantaneous power incoming into \mathbf{Q}_L through \mathbf{L}_1 (right-side's term). The instantaneous Poynting theorem (9) justifies definitions of (5) and (8). It is clear that it is possible to obtain directly the energies accumulated and dissipated in the storage unit by integrating terms 2 and 3 in (9) over a given length of time.

2.3. Frequency-domain (Spectral) Characteristics

In what follows in this section and the remainder of the paper, Fourier transform pairs are related by

$$\tilde{f}(k) = \frac{1}{2\pi} \int_0^T f(t) e^{ikt} dt \quad \leftrightarrow \quad f(t) = \int_{-\infty}^{\infty} \tilde{f}(k) e^{-ikt} dk, \quad (10)$$

where, $f(t)$ and $\tilde{f}(k)$ represent the Fourier transform pair, $k = 2\pi/\lambda$ is the wavenumber, λ is the wavelength, and T is the upper limit of the observation time.

The following frequency-domain characteristics are used together with the time-domain ones in describing the energy accumulation processes in compressors.

- (i) *Spectral Amplitude* $\tilde{U}(g, k)$ is obtained by Fourier transforming the time-domain field $U(g, t)$. When $\sigma_0(g, t) = \sigma_0(g)$ and $T \rightarrow \infty$, the function $\tilde{U}(g, k)$ is a solution of the boundary-value problem

$$\begin{aligned} [\partial_z^2 + \partial_y^2 + k^2 \tilde{\varepsilon}(g)] \tilde{U}(g, k) &= 0; \quad g = \{y, z\} \in \mathbf{Q} \\ \tilde{U}(g, t) \Big|_{g \in \mathbf{S}} &= 0. \end{aligned} \quad (11)$$

Here, $\tilde{\varepsilon}(g) = \varepsilon_r(g) + iZ_0\sigma_0(g)/k$ is the complex permittivity. Similar to their counterparts, $\tilde{U}(g, k) = \tilde{U}^i(g, k) + \tilde{U}_1^s(g, k)$ for $g \in \mathbf{I}$ and $\tilde{U}(g, k) = \tilde{U}_2^s(g, k)$ for $g \in \mathbf{II}$ and $\tilde{U}^i(g, k)$, $\tilde{U}_1^s(g, k)$, and $\tilde{U}_2^s(g, k)$ are represented in terms of modes via separation of variables [33]:

$$\begin{aligned} \tilde{U}^i(g, k) &= \sum_n \tilde{v}_{n,1}(z, k) \mu_{n,1}(y) \\ &= \sum_n b_{n,1}(k) \exp[i\gamma_{n,1}(z + L_1)] \mu_{n,1}(y); \quad g \in \mathbf{I}, \\ \tilde{U}_1^s(g, k) &= \sum_n \tilde{u}_{n,1}(z, k) \mu_{n,1}(y) \\ &= \sum_n c_{n,1}(k) \exp[-i\gamma_{n,1}(z + L_1)] \mu_{n,1}(y); \quad g \in \mathbf{I} \\ \tilde{U}_2^s(g, k) &= \sum_n \tilde{u}_{n,2}(z, k) \mu_{n,2}(y) \\ &= \sum_n c_{n,2}(k) \exp[i\gamma_{n,2}(z - L_2)] \mu_{n,2}(y); \quad g \in \mathbf{II}. \end{aligned}$$

- (ii) *Propagation Constant* of the n th waveguide mode with wavenumber k is defined as

$$\gamma_{n,j}(k) = \sqrt{k^2 - \lambda_{n,j}^2}, \quad \text{Re}\gamma_{n,j}(k) \geq 0, \quad \text{Im}\gamma_{n,j}(k) \geq 0.$$

Here, $\lambda_{n,j}$ is an eigenvalue of the waveguide **I** ($j = 1$) or **II** ($j = 2$). $\gamma_{n,j}(k)$ indicates if the mode is propagating ($\text{Re}\gamma_{n,j}(k) > 0$ and $\text{Im}\gamma_{n,j}(k) = 0$) or damped ($\text{Re}\gamma_{n,j}(k) = 0$ and $\text{Im}\gamma_{n,j}(k) > 0$), and $\gamma_{n,j}(k) = 0$ in the cut-off point.

- (iii) *Reflection and Transmission Coefficients* are defined as

$$R_{p,n}(k) = \frac{\tilde{u}_{n,1}(z,k)|_{z=L_2}}{\tilde{v}_{p,1}(z,k)|_{z=L_2}} = \frac{c_{n,1}}{b_{p,1}},$$

$$T_{p,n}(k) = \frac{\tilde{u}_{n,2}(z,k)|_{z=L_2}}{\tilde{v}_{p,1}(z,k)|_{z=L_2}} = \frac{c_{n,2}}{b_{p,1}}.$$

Here, $\tilde{v}_{p,1}(z,k)$ and $\tilde{u}_{n,j}(z,k)$, $j = 1, 2$ are the spectral amplitudes, i.e., Fourier transforms (see (10)) of the spatio-temporal amplitudes $v_{p,1}(z,t)$ and $u_{n,j}(z,t)$ (see (2)). The reflection coefficient $R_{p,n}(k)$ describes the amplitude of n th reflected mode (in the waveguide **I**) relative to p th incident mode (in the waveguide **I**); the transmission coefficient $T_{p,n}(k)$ describes the amplitude of n th transmitted mode (in the waveguide **II**) relative to p th incident mode (in the waveguide **I**). The reflection and transmission coefficients are used in the derivation of the frequency-domain expressions of the reflected and transmitted energy as described below.

- (iv) *Energy Coupling Between Modes*. Let the compressor be excited with the p th propagating mode with wavenumber k incident from the waveguide **I** ($\text{Im}\gamma_{p,1}(k) = 0$), then the relative reflected and transmitted energy components coupled to n th propagating (outgoing) modes in the waveguides **I** and **II** are defined as [33]

$$W_{p,n}^R(k) = |R_{p,n}(k)|^2 \frac{\text{Re}\gamma_{n,1}(k)}{\gamma_{p,1}(k)},$$

$$W_{p,n}^T(k) = |T_{p,n}(k)|^2 \frac{\text{Re}\gamma_{n,2}(k)}{\gamma_{p,1}(k)}.$$
(12)

Here, $W_{p,n}^R$ and $W_{p,n}^T$ are analogues of the time-domain energy characteristics (4) in the sense that they are suitable for the evaluation of the compressor's performance.

- (v) *Complex Eigenfrequency* $\bar{k}_n = \text{Re}\bar{k}_n + i\text{Im}\bar{k}_n$ is the complex wavenumber corresponding to the n th resonant frequency $\text{Re}\bar{k}_n$.

At the frequencies $k = \bar{k}_n$, nontrivial solutions $\tilde{U}_n(g, \bar{k}_n)$ of the homogeneous problem (11) ($\tilde{U}^i(g, k) \equiv 0$) describe possible fields freely oscillating in the resonator [21]. The imaginary part $\text{Im}\bar{k}_n$ defines the decay for the corresponding eigenoscillation — the amplitude of the corresponding eigenoscillation decreases with time t as $\exp(-t|\text{Im}\bar{k}_n|)$ [29–31].

- (vi) *Q-factor* of the fields at the working frequency is a measure of the compressor’s ability to accumulate and store energy. Higher *Q-factor* means slower decay of the accumulated energy (that might exist due to the reflection back into the feeding waveguide, or leak to the output waveguide, or conductive loss). The *Q-factor* is defined as [29–31]

$$Q = \frac{\text{Re}\bar{k}}{2|\text{Im}\bar{k}|}. \quad (13)$$

Here, $\bar{k} = \text{Re}\bar{k} + i\text{Im}\bar{k}$ is the complex working frequency of the compressor. Its real part $\text{Re}\bar{k}$ coincides with a conventional real working frequency of a compressor: $k_{work} = \text{Re}\bar{k}$, and the imaginary part $\text{Im}\bar{k}$ defines decay of the working oscillation.

Just like the time-domain, the origin of these characteristics is the energy conservation law (the Poynting theorem) for monochromatic waves. If a compressor is excited with the p th propagating mode with wavenumber k incident from the waveguide **I**, then the Poynting theorem for propagating modes of the waveguides **I** and **II** reads [33]

$$\sum_n W_{p,n}^R(k) + \sum_n W_{p,n}^T(k) = 1 - \frac{k^2}{\gamma_{p,1}} \int_{\mathbf{Q}_L} \text{Im}\tilde{\epsilon}(g) \left| \tilde{\vec{E}}(g, k) \right|^2 dV. \quad (14)$$

Here, $\tilde{\vec{E}}(g, k)$ is the spectral amplitude (the Fourier transform) of the time-domain electric field, $\vec{E}(g, t)$. It is clear that the last term in the right-hand side of (14) defines the relative part of energy dissipated due to conductive loss.

It should be noted here that for a fixed value of the wavenumber k , the number of propagating modes of the waveguides **I** and **II** is finite and given by $M_j = \sum_n (\text{Re}\gamma_{n,j}/|\gamma_{n,j}|)$, $j = 1, 2$ (for propagating modes $\text{Im}\gamma_{n,j} = 0$, then $\text{Re}\gamma_{n,j}/|\gamma_{n,j}|$ is either zero or one). Let M be the number of propagating modes inside the storage unit, then the set $\{M_1, M_2, M\}$ can be used to name the compressor’s regime of operation [33]. For example, if $\max\{M_1, M_2\} = N$, then the regime of operation is called “ N -modes” regime, if $M_1 < M$ and $M_2 < M$, then it is called the “trapped modes” regime.

3. COMPRESSOR DESIGN AND ENERGY ACCUMULATION

In this section, the energy accumulation process is described in detail; and the influence of the compressor's geometric parameters, (conductive) absorption in the storage unit's walls, and the parameters of excitation (frequency, duration) on the energy accumulation process and the compressor's overall performance is characterized. In addition, a method to set the optimal excitation duration is discussed. For this purpose, a model compressor constructed from rectangular waveguides is considered. It is assumed that the feeding waveguide of compressor is excited by $TE_{0,n}$ waves ($E_y = E_z = H_x = 0$, the first index determines the number of field peaks in the x direction, the second one — in the y direction). Under this assumption, since there is no field variation in the x direction, the compressor under study is accurately modelled using the 2-D structure in the $y0z$ plane (Fig. 1). The electromagnetic wave interactions on this structure are described by the initial-boundary value problem (1) (see Section 2.1), where $U(g, t) = E_x(g, t)$. It should be noted here that, for more general cases and more complicated structures, three-dimensional (3-D) models are needed to accurately model all aspects of the pertinent physics. In such cases, only the electromagnetic initial-boundary value problem will be different; however, the discussions on the design principles and the energy accumulations characteristics described here would be unchanged. Before presenting the details of the energy accumulation processes on the model compressor in the rest of this section, a brief summary of the design scheme and the material that will be detailed in the subsequent sections is given below:

First, prototypes for the compressor's storage unit, feeding and output waveguides are chosen. Waveguide cavity resonator is coupled with a feeding waveguide via a thin beyond-cutoff diaphragm. The geometric parameters of the storage unit and the waveguides are set to enable the propagation of certain modes and to get the desired Q -factor.

The complex eigenfrequencies $\bar{k}_n = \text{Re}\bar{k}_n + i\text{Im}\bar{k}_n$ of the storage unit are computed, the Q -factors and the field patterns of corresponding eigenoscillations are determined. One of the values of $\text{Re}\bar{k}_n$ is chosen as the working frequency of compressor, k_{work} . The choice is made taking into account two factors: (i) The Q -factor of oscillation at $k_{work} = \text{Re}\bar{k}_n$, as it defines the energy efficiency of compressor. (ii) The remoteness of k_{work} from the real values of eigenfrequencies of the compressor with open output waveguide, as this parameter together with the length of storage unit define duration

of the compressed pulse (the compressor with open output waveguide should not resonate in the neighborhood of the working frequency k_{work}).

The switch that locks/unlocks the output waveguide at the frequency k_{work} is designed. The switch is integrated with the open output waveguide in such a way that the structure of the storage unit + the short-circuited output waveguide and the structure of the storage unit + the locked switch + the open output waveguide sustain exactly the same oscillation at the frequency k_{work} .

The process of energy accumulation is studied in detail. Influence of the switch, the size of the coupling window between the feeding waveguide and the storage unit, the conductive wall loss and the excitation's frequency on the compressor's performance is discussed. The (time- and frequency-domain) characteristics of the compressor are computed for quasi-monochromatic pulses of various durations, and the optimal duration of excitation is set in accordance with the compressor's specification.

3.1. Initial Prototype

The geometrical parameters of the rectangular storage unit, feeding and output waveguide are chosen such that, in the frequency band of interest $3.2 < k < 4.1$ rad/m, the feeding waveguide supports only $TE_{0,1}$ mode, and the storage unit and the output waveguide support only three $TE_{0,n}$, $n = 1, 2, 3$ modes. This choice sets the parameters as $a_2 = 3.0$ m, $d_2 = 10.0$ m, $d_3 = 3.0$ m and $a_1 = 1.28$ m, $d_1 = 3.0$ m (Fig. 1). The storage unit is coupled with the feeding waveguide via a thin beyond-cutoff diaphragm with $d = 0.06$ and $a = 0.4$ [21, 33–36]. The virtual boundaries \mathbf{L}_1 and \mathbf{L}_2 are set at $z = -L_1 = 0.0$ and $z = L_2 = 16.0$ m, respectively. A distributed grating-type switch is used in the compressor design under study [16]. It is a periodic system of quartz discharge tubes (see Fig. 1, the diameter of the tube $h = 0.4$ m, the period $l = 0.6$ m, the thickness of the walls is 0.02 m, and the permittivity of the quartz walls is $\varepsilon_r = 3.8$).

3.2. Determining the Working Frequency

The working frequency of the compressor is chosen from the eigenfrequencies of the storage unit. This is performed in two steps: (i) The eigenfrequencies of the short-circuited compressor (the compressor with the closed output waveguide) are extracted from the frequency-domain response obtained from a time-domain simulation with broadband excitation. Similarly, eigenfrequencies of the compressor with the open output waveguide are computed.

The eigenfrequencies obtained in the first and second simulations are compared; the eigenfrequencies of the short-circuited compressor, which are not within the neighborhood of any of the eigenfrequencies of the compressor with the open output waveguide, are chosen. (ii) For each of those eigenfrequencies, a more precise (narrowband) simulation is performed to find the eigenfrequency with the highest Q -factor.

To obtain the broadband response in time-domain, the short-circuited compressor is excited with a broadband Gaussian $TE_{0,1}$ pulse. This excitation is implemented by setting $U^i(g, t) = E_x^i(g, t)$: $v_{1,1}(0, t) = F_1(t) = \exp[-(t - \bar{T})^2/4\alpha^2] \cos[\tilde{k}(t - \bar{T})] \chi(\bar{T} - t)$. Here, $v_{1,1}(0, t)$ represents the amplitude of the pulse on the virtual boundary \mathbf{L}_1 ($z = -L_1 = 0$) (see (2)), $\chi(\cdot)$ is the Heaviside step function and the parameters \bar{T} , \tilde{T} , \tilde{k} , and α are the duration, delay, modulation (center) frequency, and the bandwidth of the pulse, respectively. These parameters are chosen as $\bar{T} = 30$ m, $\tilde{T} = 15$ m, $\tilde{k} = 3.5$ rad/m, and $\alpha = 2$; this choice of parameters results in $F_1(t)$ and its Fourier transform $\tilde{F}_1(k)$ that are plotted in Fig. 2(a). The total observation time $T = 1000$ m is long enough to allow the oscillations in compressor to reach a steady-state. The snapshot of the time-domain fields induced in the compressor at $t = 804.5$ m is given in Fig. 3(a). The antinodal point $g_1 = \{y = 0, z = 12.3\}$ is clearly marked in the same figure. The normalized spectrum at point g_1 , $|\tilde{U}(g_1, k, T)|$, is obtained by Fourier transforming the free-oscillating (in the absence of excitation, $\bar{T} < t \leq T$) time-domain field $U(g_1, t)$, to obtain $\tilde{U}(g_1, k)$ and subsequently dividing $\tilde{U}(g_1, k)$ by the Fourier transform of the excitation's time signature, $\tilde{F}_1(k)$. The values of real parts $\text{Re}\bar{k}$ of complex eigenfrequencies \bar{k} are identified as $\text{Re}\bar{k} = \{3.345, 3.52, 3.65, 3.675, 3.85, 3.953, 4.04\}$ from the resonance peaks in normalized spectrum $|\tilde{U}(g_1, k, T)|$ (see Fig. 3(b)). A similar simulation is performed on the compressor with the open output waveguide and its eigenfrequencies are found to be $\text{Re}\bar{k} = \{3.3, 3.4, 3.51, 3.62, 3.73, 3.88\}$. Each of the eigenfrequencies of the short-circuited compressor, which are remote enough from the eigenfrequencies of the compressor with the open output waveguide, namely $\text{Re}\bar{k} = \{3.675, 3.85, 3.953, 4.04\}$, are studied more carefully in the next step.

The Q -factors and field patterns of the eigenoscillations are determined from a set of simulations with narrowband Gaussian excitation with $v_{1,1}(0, t) = F_1(t)$ where now $\alpha = 20$, $\tilde{T} = 100$ m, $\bar{T} = 200$ m. At each simulation the center frequency of the excitation, \tilde{k} , is set to one of the eigenfrequencies obtained as a result of the initial broadband simulation, $\tilde{k} = \{3.675, 3.85, 3.953, 4.04\}$. This

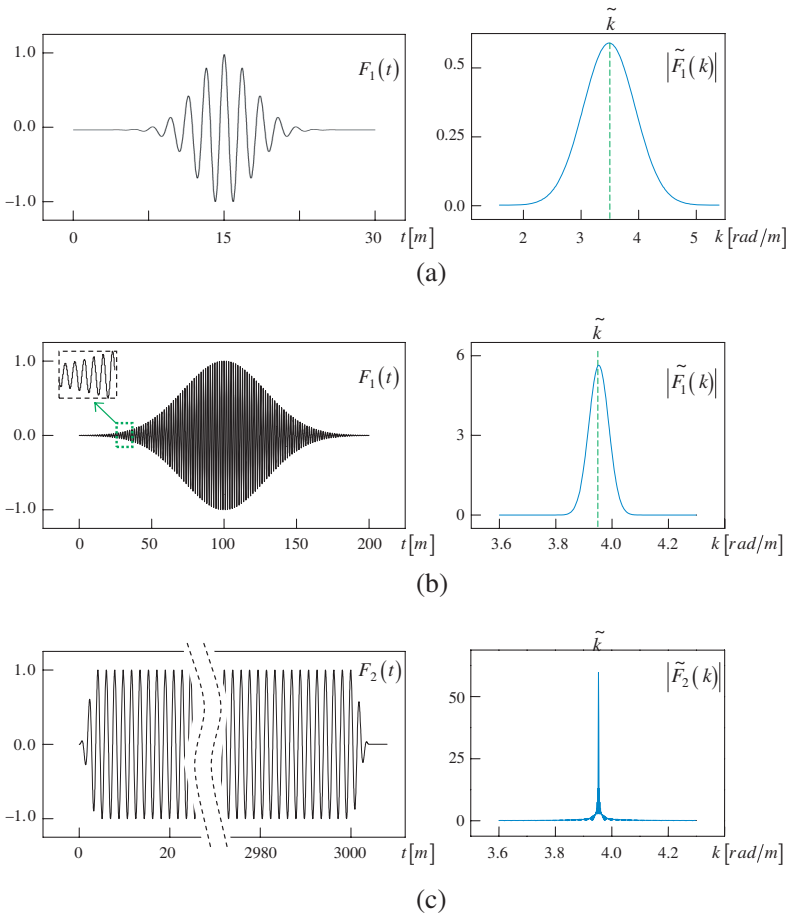


Figure 2. Temporal and spectral characteristics of excitation pulses. (a) Broadband Gaussian pulse: $v_{1,1}(0, t) = F_1(t)$, $\tilde{k} = 3.5$ rad/m, $\alpha = 2$, $\tilde{T} = 15$ m, $\bar{T} = 30$ m. (b) Narrowband Gaussian pulse: $v_{1,1}(0, t) = F_1(t)$, $\tilde{k} = 3.953$ rad/m, $\alpha = 20$, $\tilde{T} = 100$ m, $\bar{T} = 200$ m. (c) Long quasi-monochromatic pulse: $v_{1,1}(0, t) = F_2(t)$, $\tilde{k} = 3.953$ rad/m, $t_{start} = 0.1$ m, $t_{oneL} = 5$ m, $t_{oneR} = 3000$ m, $t_{end} = 3004.9$ m.

choice of parameters ($\tilde{k} = 3.953$ rad/m) results in $F_1(t)$ and its Fourier transform $\tilde{F}_1(k)$ that are plotted in Figs. 2(b). In these simulations, the observation time is set as $T = 600$ m to allow the eigenoscillations to reach steady state. The Q -factor at each of these frequency points is obtained by studying the free-oscillating (in the absence of the

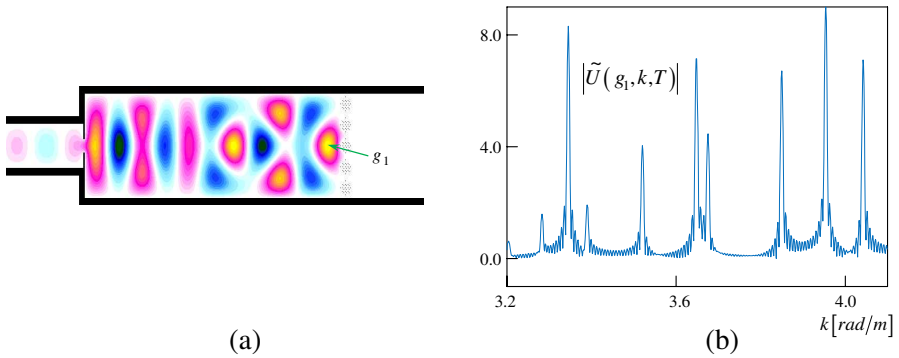


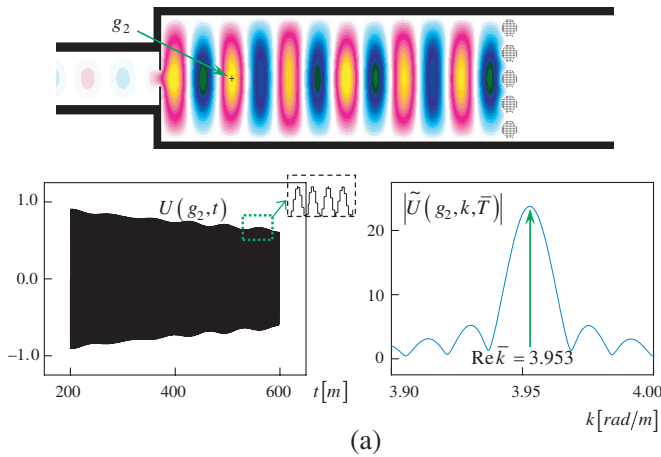
Figure 3. Excitation of the compressor by the broadband Gaussian pulse: (a) Field pattern of E_x component at the instant of time $t = 804.5$ m (free oscillations); (b) Normalized spectrum of the free-oscillating field in the antinodal point g_1 .

excitation, $\bar{T} < t \leq T$) field $U(g_2, t)$ and its spectral amplitude $\tilde{U}(g_2, \tilde{k})$, which is obtained by Fourier transforming $U(g_2, t)$; here g_2 represents an antinodal point in a given simulation (see the first plot in Fig. 4(a) the antinodal point $g_2 = \{y = 0, z = 5.04\}$ for the simulation with $\tilde{k} = 3.953$ rad/m). As it is shown in [29–31], the envelope of the amplitude of free-oscillating field decreases with time t as $\exp(-t|\text{Im}\bar{k}|)$, so the value of $|\text{Im}\bar{k}|$ can be found (see the second plot in Fig. 4(a) for the decaying oscillations of $U(g_2, t)$ at $\tilde{k} = 3.953$ rad/m; for this simulation $\text{Im}\bar{k} = -0.0003$). Once $|\text{Im}\bar{k}|$ is found, Q -factor at each frequency is computed using (13); the highest Q -factor $Q \approx 6600$ is obtained for the simulation with $\tilde{k} = 3.953$ rad/m. This frequency is chosen as the working frequency $k_{work} = 3.953$ rad/m.

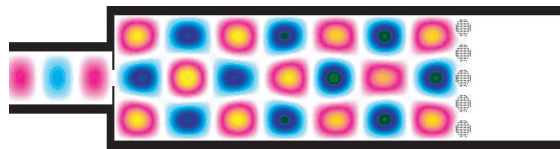
For the sake of completeness the snapshots of the field distributions at $t = 210.5$ m for the simulations with $\tilde{k} = 3.953$ rad/m, $\tilde{k} = 3.85$ rad/m, and $\tilde{k} = 4.04$ rad/m are presented in Figs. 4(a), (b) and (c), respectively. It should be observed that $\text{Re}\bar{k} = 3.953$, $\text{Re}\bar{k} = 3.85$, and $\text{Re}\bar{k} = 4.04$ correspond to $TE_{0,1,12}$, $TE_{0,3,7}$, and $TE_{0,3,8}$ modes respectively.

3.3. Energy Accumulation Process in Details

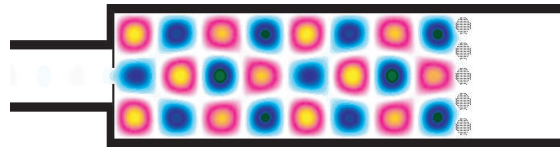
The full information on the energy accumulation in the compressor is obtained exciting the compressor with a long quasi-monochromatic $TE_{0,1}$ pulse and studying the behavior of the mode amplitudes $u_{1,1}(z, t)$ and $u_{1,2}(z, t)$ (see (2) for their definitions) on the virtual boundaries



(a)



(b)



(c)

Figure 4. Excitation of the compressor by the narrowband Gaussian pulse with varying central frequency $\tilde{k} = \text{Re}\bar{k}$: (a) $\tilde{k} = 3.953$ rad/m; (b) $\tilde{k} = 3.85$ rad/m; (c) $\tilde{k} = 4.04$ rad/m. All field patterns are shown at the instant of time $t = 210.5$ m (free-oscillations, E_x component).

L_1 and L_2 , and the total field, $U(g, t)$, inside the compressor. The quasi-monochromatic excitation is implemented by setting $v_{1,1}(0, t) = F_2(t) = \text{Tr}(t) \cos(\tilde{k}t)$. Here, $\text{Tr}(t)$ represents a trapezoidal envelope which is equal to zero for $t < t_{start}$ and $t > t_{end}$, and is equal to one for $t_{oneL} < t < t_{oneR}$, the central frequency \tilde{k} coincides with the working frequency k_{work} (Fig. 2(c)).

Indeed, the amplitudes $u_{1,1}(0, t)$ and $u_{1,2}(L_2, t)$ of reflected and transmitted pulses shows how much energy is reflected back into the feeding waveguide and leak into the output waveguide through the

switch during the accumulation of energy. These amplitudes are used to determine the instantaneous energy accumulation efficiency $\eta_{accum}(t)$ (see (8) for the definition). The efficiency of energy accumulation is relatively high for periods of time when the amplitudes $u_{1,1}(0, t)$ and $u_{1,2}(L_2, t)$ are relatively small and vice versa.

As expected, the amplitude $u_{1,2}(L_2, t)$ depends mostly on the properties of the switch; in Section 3.3.1, it is used to quantify the effect of the switch on the performance of the compressor. The amplitude $u_{1,1}(0, t)$ depends mostly on the size of the coupling window; in Section 3.3.2, the optimal window size is determined by minimizing the reflection into the feeding wave guide via investigation of the behavior of $u_{1,1}(0, t)$.

The total field $U(g, t)$ evaluated at the antinodal point g_2 describes the behavior of the working oscillation in the storage unit, and hence, determines the amplitude of the compressed (output) pulse and its rate of increase. Higher maximum amplitude means that more energy could be accumulated in the storage unit, and hence, the bigger power gain is possible. As described in Section 3.3.3, investigating the behavior of $u_{1,1}(0, t)$, $u_{1,2}(L_2, t)$ and $U(g_2, t)$ is used in determining the optimal duration of excitation.

3.3.1. Switch

As mentioned earlier, a distributed grating-type switch is used in the compressor. A properly designed switch should not affect the performance of the overall compressor design. To verify that the switch satisfies this requirement, one can compute the frequency-domain energy characteristics $W_{1,n}^R(k)$ and $W_{1,n}^T(k)$ for two modes of operation of the switch and investigate if it behaves as expected: (i) Energy accumulation: The switch is closed, the tubes are on; they are filled with plasma with $\varepsilon_r = 1.0$ and $\sigma_0 = 5.7 \cdot 10^4$ S/m. (ii) Energy exhaust: The switch is unlocked, the tubes are off; they are filled with a gas with $\varepsilon_r = 1.0$ and $\sigma_0 = 0$. In both simulations the switch (see insets in Fig. 5) is excited with the broadband Gaussian pulse $U^i(g, t)$: $v_{1,1}(0, t) = F_1(t)$ with $\tilde{k} = 3.5$ rad/m, $\tilde{T} = 15$ m, $\bar{T} = 30$ m, and $\alpha = 2$. $W_{1,n}^R(k)$ and $W_{1,n}^T(k)$ are obtained from the Fourier transformed broadband time-domain results (see Section 2.3). Figs. 5(a) and (b) present $W_{1,n}^R(k)$ for (i) and $W_{1,n}^T(k)$ for (ii) $n = 1, 2, 3$, respectively. As demonstrated by these figures, the switch works exactly as expected: (i) it does not lead to unwanted mode coupling ($W_{1,n}^R(k) = 0$ and $W_{1,n}^T(k) = 0$ for $n = 2, 3$), (ii) the output waveguide is completely closed during the energy accumulation (Fig. 5(a): $W_{1,1}^R(k) \approx 1$), and

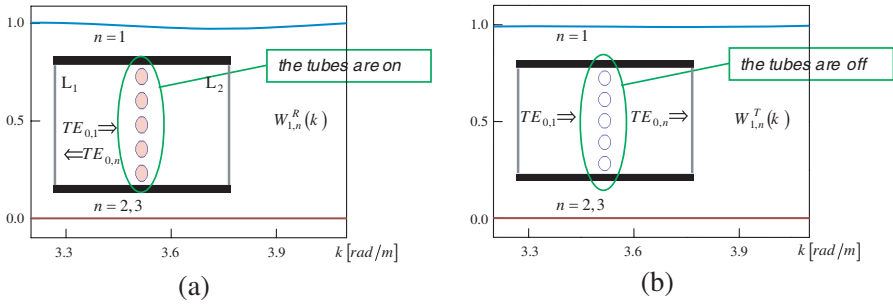


Figure 5. Electrodynamics characteristics of the switch: (a) during the accumulation of energy (the discharge tubes are on, the switch is locked); and (b) during the exhaust (the discharge tubes are off, the switch is unlocked).

(iii) the output waveguide is completely open during the energy exhaust (Fig. 5(b): $W_{1,1}^T(k) \approx 1$).

One may expect that the amplitude $u_{1,2}(L_2, t)$, which determines the amount of energy that leaks into the output waveguide through the switch, is constant in time, but the Fig. 6 clearly shows that it is not true. The amplitude $u_{1,2}(L_2, t)$ also depends on the amount of energy accumulated in the compressor (compare $u_{1,2}(L_2, t)$ and $U(g_2, t)$ in Fig. 6). This means that the performance of the switch should be monitored during the whole period of energy accumulation, and confirms importance of the time-domain studies. It should be noted here that in all the cases shown in Fig. 6, $u_{1,2}(L_2, t)$ is vanishingly small during the energy accumulation, which confirms that the switch was designed properly.

3.3.2. Determining the Coupling Window Size

The size of coupling window a affects the compressor's complex eigenfrequencies [33, 35, 36], but changing a has a bigger effect on the imaginary part of the eigenfrequencies rather than their real parts. This can be explained by the fact that a determines the amount of energy reflected back into the feeding waveguide (the amplitude $u_{1,1}(0, t)$), and thus, the working oscillation's attenuation. This means that, if the size of coupling window is fixed (i.e., when the Q -factor is fixed), the only parameter that can change the instantaneous energy accumulation efficiency $\eta_{accum}(t)$ is the duration of the excitation. A behavior of this (non-monotonic) dependence in general is the same for storage units with different sizes of coupling windows (and, thus, different Q -factors). The increase of Q -factor results in an increase of

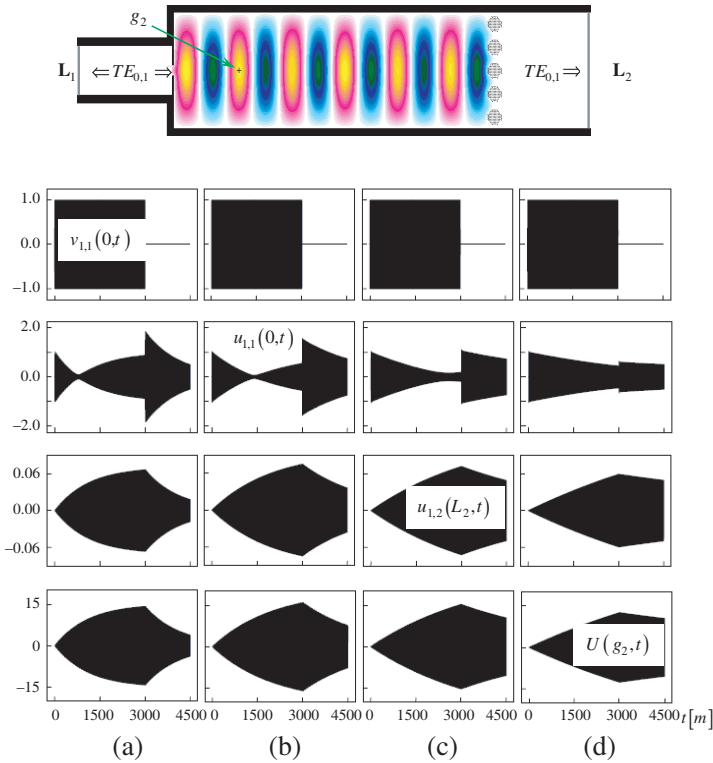


Figure 6. Excitation of the compressor with varying size of the coupling window a by a long quasi-monochromatic pulse with varying central frequency \tilde{k} : (a) $a = 0.4$ m, $\tilde{k} = 3.953$ rad/m; (b) $a = 0.36$ m, $\tilde{k} = 3.9546$ rad/m; (c) $a = 0.32$ m, $\tilde{k} = 3.95625$ rad/m; (d) $a = 0.28$ m, $\tilde{k} = 3.9575$ rad/m.

limiting value of amplitude of $U(g_2, t)$ (and hence, the output pulse's amplitude also) and leads to extension of the excitation time required to achieve the same value of $\eta_{accum}(t)$ (it takes longer to reach higher limiting value of $U(g_2, t)$).

To find the optimal size of coupling window a , which would minimize the reflection into the feeding waveguide and maximize the Q -factor, first $\bar{k} = \text{Re}\bar{k} + i\text{Im}\bar{k}$, which correspond to complex eigenfrequencies of the compressors with various a 's are computed as described in Section 3.2 (the real parts of the eigenfrequencies only slightly differ from $k_{work} = 3.953$ rad/m); then the compressor in the each case is excited with the long quasi-monochromatic pulse: $v_{1,1}(0, t) = F_2(t)$. The parameters of this excitation are set as $\tilde{k} = \text{Re}\bar{k}$,

$t_{start} = 0.1$ m, $t_{oneL} = 5$ m, $t_{oneR} = 3000$ m, $t_{end} = 3004.9$ m. Among the cases whose simulation results are shown in Fig. 6, the combination of the coupling window size $a = 0.32$ m and the frequency $\text{Re}\bar{k} = 3.95625$ rad/m (Fig. 6(c)) is an optimal choice as it provides minimal reflection into the feeding waveguide (note the behavior of $u_{1,1}(0, t)$), perspective of further growth of the amplitude of working oscillation with increasing length of the excitation (note the fast growth of $U(g_2, t)$ before the excitation is turned off at $t = 3005$ m) and the highest Q -factor (note the slow decay of $U(g_2, t)$ after the excitation is turned off). So, from here on the size of coupling window and the working frequency are set fixed as $a = 0.32$ m and $k_{work} = 3.95625$ rad/m, respectively.

The results presented above demonstrate the importance of the rigorous full-wave time-domain methods over the simplified schemes, which use simplified models for the coupling window [8, 12] and do not take into account all the time-dependent factors, such as dependence of the amount of energy reflected back into the feeding waveguide on the amount of energy accumulated in storage unit. The method presented here obviously takes into account the non-monotonic time dependence of the accumulation processes.

3.3.3. Setting the Duration of Excitation

When the amplitude of $U(g_2, t)$ stops growing, this means that the compressor cannot intake any more energy. Energy pumping from the input after this point results in a significant reduction of the compressor's overall efficiency η since this will result in the total reflection of the input back into the feeding waveguide. Thus, in the case when the highest possible power gain θ (see (7) for the definition) is desired, the excitation should be turned off when the amplitude of $U(g_2, t)$ reaches its maximum. On the other hand, it is possible to trade high θ for high η : note that the behavior of $u_{1,1}(0, t)$ is non-monotonic — for example, in Fig. 6(b) it decreases for $0 < t < 1500$ m and then it increases until the excitation is turned off at $t = 3000$ m. If the excitation is turned off soon after the moment when $u_{1,1}(0, t)$ reaches its minimum value, then both $\eta_{accum}(t)$ and η stay high. Examination of the behavior $\eta_{accum}(t)$ can provide the optimal duration of the excitation to maximize η — the excitation should be turned off at the moment when $\eta_{accum}(t)$ reaches its maximum value.

To find the optimal duration of excitation the compressor is excited with a long quasi-monochromatic pulse: $v_{1,1}(0, t) = F_2(t)$ with $\tilde{k} = k_{work} = 3.95625$ rad/m, $t_{start} = 0.1$ m, $t_{oneL} = 5$ m, $t_{oneR} = 10\,100$ m, $t_{end} = 10\,104.9$ m. An auxiliary variable, the

normalized field intensity of working oscillation in antinodal point, is introduced as $\alpha(t) = \frac{\max_{0 < \tau \leq t} |U(g_2, \tau)|}{\max_{\tau > 0} |U(g_2, \tau)|}$. Table 1 shows the values of $\eta_{accum}(t)$, $\alpha(t)$ and θ at the distinguished instants of time: around $t = 2500$ m there is almost no reflection back into the feeding waveguide (Fig. 7(b)); around $t = 5000$ m $\eta_{accum}(t)$ reaches its maximum; $t = 7500$ m is a midpoint between maximum efficiency and maximum field intensity; around $t = 10000$ m $\alpha(t)$ (and, correspondingly, $U(g_2, t)$) reaches its maximum (Fig. 7(c)).

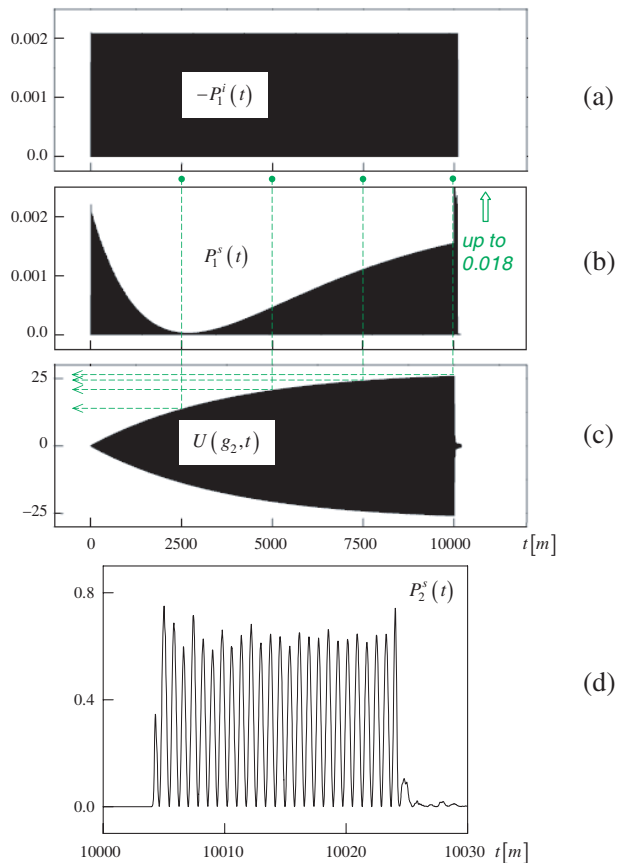


Figure 7. Accumulation and exhaust of the energy: (a) Instantaneous power of the excitation; (b) Instantaneous power of the wave reflected back into the waveguide **I**; (c) Electric field (E_x component) intensity in the antinodal point g_2 ; (d) Instantaneous power of the compressed pulse.

Table 1. Energy accumulation efficiency, normalized field intensity and power gain at the distinguished instants of time.

	$t = 2500$ m	5000 m	7500 m	10 000 m
$\eta_{accum}(t)$	0.691	0.8	0.736	0.637
$\alpha(t)$	0.509	0.774	0.906	0.981
$\theta(t)$ for $T^i = t$	78	181	251	290

If high θ is desired, then the excitation should be turned off when $U(g_2, t)$ reaches its maximum and is not increasing any more. According to Fig. 7(c) and Table 1, this happens around $t = 10\,000$ m. On the other hand, if high η is desired, the excitation should be turned off when $\eta_{accum}(t)$ reaches its maximum, which happens around $t = 5000$ m according to Table 1 (by this time the amplitude of $U(g_2, t)$ reaches only 0.774 of its maximum). Assuming that high θ is required, $t = T^i = 10000$ m is set as the time instant when the excitation is turned off.

3.3.4. Influence of the Excitation Frequency on the Compressor's Performance

For proper operation of the compressor, it is important to set precisely the frequency of the pulse to the working frequency of the compressor. Even a small deviation from the working frequency results in a complete loss of ability to accumulate energy in the storage unit. To demonstrate this, two simulations are performed. In both simulations, the same compressor is excited with the quasi-monochromatic pulse $U^i(g, t): v_{1,1}(0, t) = F_2(t)$ with $t_{start} = 0.1$ m, $t_{oneL} = 5$ m, $t_{oneR} = 5000$ m, $t_{end} = 5004.9$ m; however in the first simulation $\tilde{k} = \tilde{k}_1 = 3.95625$ rad/m, while in the second simulation $\tilde{k} = \tilde{k}_2 = 3.953$ rad/m. Note that \tilde{k}_1 fully agrees with k_{work} up to the fifth digit, while \tilde{k}_2 agrees with k_{work} up to the second digit only. A comparison of $u_{1,1}(0, t)$ in Fig. 8(a) (obtained in the first simulation) with $u_{1,1}(0, t)$ in Fig. 8(b) (obtained in the second simulation) clearly demonstrates that in the second simulation the compressor turns into a well reflecting inhomogeneity. In the second simulation there is almost no difference between the amplitudes of input and reflected pulses which means that almost all input energy is reflected back into the feeding waveguide. In addition, a comparison of $U(g_2, t)$, field values evaluated at the antinodal point $g_2 = \{y = 0, z = 5.04\}$ (Figs. 8(a) and (b)), reveals that in the second simulation the amplitude of the field in the storage unit is not growing, and, thus, the compressor does not accumulate energy.

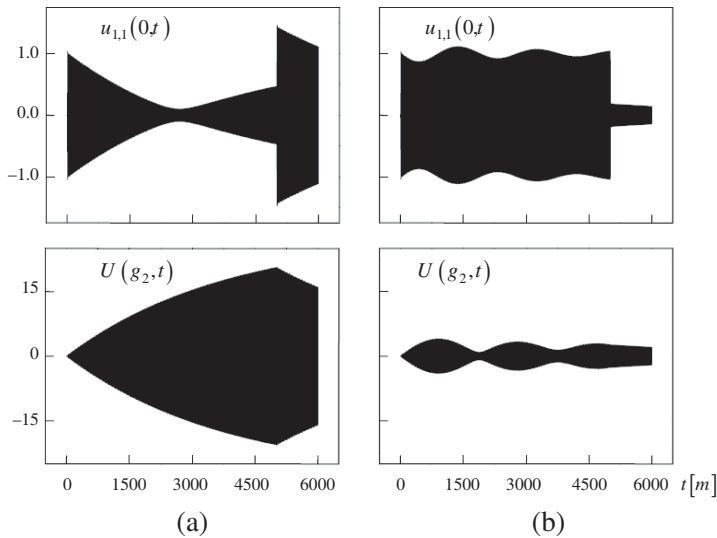


Figure 8. Influence of the central frequency \tilde{k} of the excitation pulse on the compressor’s ability to accumulate energy: (a) The central frequency coincides exactly with the working one $\tilde{k} = k_{work} = 3.95625$ rad/m; (b) The central frequency is slightly incorrect $\tilde{k} = 3.953$ rad/m.

3.3.5. Influence of the Wall Loss on the Compressor’s Performance

The design and analysis above is performed assuming that the walls of the compressor are PEC. To make the model more realistic, and quantify the effects of this on the results, a compressor with walls constructed from non-perfectly conducting metal is studied. To model the effect of the loss, PEC walls from inside are inlaced with a 0.02 m thick layer of copper ($\epsilon_r = 1.0$, $\sigma_0 = 5.7 \cdot 10^7$ S/m), see Fig. 9(a). This more “realistic” compressor is excited with the quasi-monochromatic pulse $U^i(g, t): v_{1,1}(0, t) = F_2(t)$ with $\tilde{k} = 3.95625$ rad/m, $t_{start} = 0.1$ m, $t_{oneL} = 5$ m, $t_{oneR} = 5000$ m, $t_{end} = 5004.9$ m. Introduction of the lossy layer does not lead to any visible difference in the processes of energy accumulation (compare Figs. 9(b)–(e) with Fig. 6(c) or with Fig. 8(a), but note that in the cases presented in Fig. 6 the duration of excitation is shorter). The introduction of the lossy layer changes negligibly the eigenfrequency of the storage unit (because the geometrical parameters of the storage unit are affected), but the important fact is that the walls loss does not affect essentially the energy accumulation process.

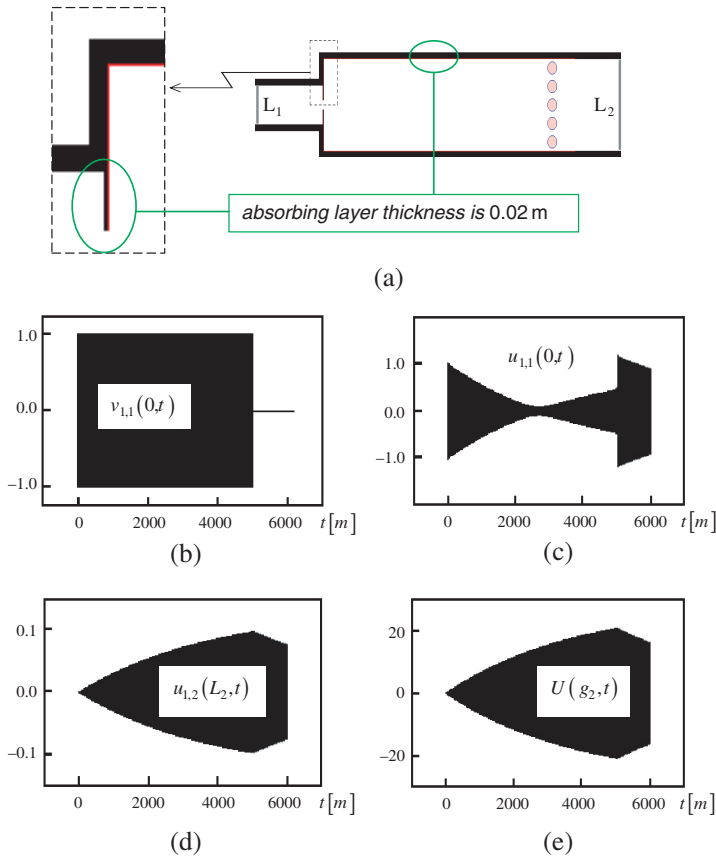


Figure 9. Compressor with the absorbing walls excited by a long quasi-monochromatic pulse: (a) Geometry of the compressor; (b)–(d) Amplitudes of the incident, reflected and transmitted pulses on the virtual boundaries L_1 ($z = 0$) and L_2 ($z = L_2$); (e) Electric field (E_x component) intensity in the antinodal point $g_2 = \{y = 0, z = 5.04\}$.

3.4. Final Design and Discussions on Performance

Finally, setting $TE_{0,1,12}$ oscillation on the frequency $k_{work} = 3.95625$ rad/m as the working one, the Q -factor of the compressor is determined: $Q = 7912.5$ (see (13), $\text{Re}\bar{k} = 3.95625$ and $\text{Im}\bar{k} = -0.00025$). The duration of excitation is set as $T^i = 10000$ m, and the switch operates as following: until the instant of time $t = 10000$ m it is locked, and starting from $t = 10001$ m it is unlocked. On the short time interval $10000 \leq t \leq 10001$ the specific conductivity of the

medium inside the discharge tubes changes from $\sigma_0 = 5.7 \cdot 10^4$ S/m down to $\sigma_0 = 0$. The whole compressor operates as following: during the energy accumulation interval $0 < t < 10000$ m it is excited with the long quasi-monochromatic pulse $U^i(g, t)$: $v_{1,1}(0, t) = F_2(t)$ with $\tilde{k} = k_{work}$, $t_{start} = 0.1$ m, $t_{oneL} = 5$ m, $t_{oneR} = 9995$ m, $t_{end} = 10000$ m, the excitation ends at the moment of time $t = T^i = 10000$ m, the switch unlocks and a high-power short RF pulse is exhausted into the output waveguide through the virtual boundary \mathbf{L}_2 during the time $T_2^s \approx 10025.5 - 10004 = 21.5$ m (Fig. 7(d)). The duration of the output (compressed) pulse T_2^s is a little longer than double length of the storage unit d_2 (see Fig. 1), it is expected as the compressor with unlocked switch is not a resonant structure and all the accumulated energy immediately released. It should be noted here that during the exhaust interval $10004 < t < 10025.5$ m the amplitude of the instantaneous power of the compressed pulse $P_2^s(t)$ is 325 times and 16250 times higher than the maximum amplitudes of the instantaneous powers $P_1^i(t)$ and $P_2^s(t)$ (associated with the excitation and the pulse seeped out into the output waveguide) during the energy accumulation interval $0 < t < 10000$ m (Fig. 7).

Thus, for the compressor with the storage unit's length of $d_2 = 10.0$ m (see Fig. 1), the working frequency $k_{work} = 3.95625$ rad/m (the working wavelength $\lambda_{work} \approx 1.588$ m), the following characteristics are obtained: the optimal duration of excitation for the highest power gain $T^i = 10000$ m = $33.3564 \mu\text{s}$, the duration of compressed output pulse $T_2^s = 21.5$ m = 71.7163 ns, the degree of compression $\beta = T^i/T_2^s \approx 465$, the efficiency $\eta = W_2^s(10004; 10025.5)/W_1^i(0; T^i) \approx 0.6238$, the power gain $\theta = \beta \cdot \eta \approx 290$. The compressor's efficiency η is a bit smaller than the efficiency of energy accumulation $\eta_{accum}(T^i)$ because a fraction of the accumulated energy is distributed among the short intensive spike in the reflected signal and the tail following the main output pulse. It should be noted here that due to the scalability of the Maxwell's equations, it is straightforward to transfer the results obtained using the scheme presented in this paper to any other geometrically similar structure. If the frequency is increased by a certain factor, then the (spatial) dimensions of the geometries and the time t (as it is measured in meters) should be divided by that factor to obtain the same results.

It should be emphasized here that the rigorous real-time study of the energy accumulation and exhaust processes allows precise adjustment of the critical parameters of a compressor (such as geometry of a coupling window (see Section 3.3.2), excitation frequency (see Section 3.3.4) and duration of excitation (see Section 3.3.3)) to obtain maximum efficiency or power gain. This is one of the advantages of the presented time-domain rigorous modeling-based approach, as

parameters of a model could be changed on the fly and effects of these changes could be obtained with high accuracy. Such optimization might be hard to achieve using simplified theories or experimental-based approach.

Having said that, the final characteristics given above may seem overoptimistic, when compared to experimental findings presented in [2, 10–12, 14] for similar types of compressors. This difference can mainly be attributed to the difference between the excitation durations; a relatively long duration of excitation is used in this paper, which naturally results in rather high values of the degree of compression and the power gain for high- Q cavities. It should be noted here that this duration is found to be optimal to obtain the highest power gain; in the experimental results, such long duration might have not been employed due to practical limitations of the generators. If the duration of excitation in the example presented above is reduced, it can be observed that the characteristics will get closer to the ones obtained experimentally.

4. BRIEF DESCRIPTION OF THE NUMERICAL TECHNIQUE

It can be concluded without hesitation that this paper demonstrates the advantages of the time-domain analysis over its frequency-domain (steady-state) counterpart for the design of microwave compressors. In this work, because of this reason, FDTD method is used for characterizing transient energy accumulation in compressors.

To enable the use of FDTD methods for solving the open initial-boundary value problem, which mathematically models the wave interactions on compressors (Section 2.1), the computation domain has to be truncated. Traditional methods involving perfectly matched layers and approximate absorbing boundary conditions [37] cannot be used in this work because of the enormous length of the simulation times needed to observe weakly-decaying highly-oscillatory fields (the number of time steps can easily exceed 1000000); these methods will simply introduce numerical error build up for such long simulation times. To ensure the reliability of the final results at the end of long time marching, exact absorbing conditions (EACs) proposed in [19–21] are utilized here. These conditions are derived using rigorous mathematical manipulations and consequently are mathematically exact. Papers [19, 20] focus on the derivation EACs for axially symmetric and 2-D plane-parallel waveguide problems, respectively. Paper [19] also describes a blocked FFT-based scheme for reducing the computational cost of the temporal convolutions present in non-local

EACs to $O(T \log^2 T)$ from $O(T^2)$. It should be noted here that this acceleration scheme is numerically exact.

These two advanced techniques, namely EACs and the blocked FFT-acceleration scheme, when combined with FDTD method, enable the accurate and efficient analysis of weakly-decaying highly-oscillatory transients on compressors. In addition, real-time observation capability that comes with any time domain method renders the FDTD method with FFT-accelerated EACs a preferred design tool for engineers.

5. CONCLUSION

It is impossible to design a microwave energy compressor without in-depth understanding of the non-monotonic physical behavior of the highly resonant high power pulses present in the storage unit. This can successfully be achieved by a design scheme that heavily depends on time-domain analysis. In this work, practically for the first time, all physical processes inside a microwave energy compressor are studied in time-domain in detail from the very beginning of the excitation right until the end of the accumulated energy's exhaust. Additionally, effects of compressor's design and excitation parameters on performance of compressor are quantified.

The methodology and the results presented here are valuable in design and fabrication of microwave compressors. In Part II of this paper, the methodology developed here will be used to design a novel combined compressor/radiator antenna element for a phased array.

REFERENCES

1. Bossart, R., P. Brown, J. Mourier, I. V. Syratchev, and L. Tanner, "High-power microwave pulse compression of klystrons by phase-modulation in high- Q storage cavities," *CERN CLIC-Notes*, No. 592, 2004.
2. Vikharev, A. L., O. A. Ivanov, A. M. Gorbachev, S. V. Kuzikov, V. A. Isaev, V. A. Koldanov, M. A. Lobaev, J. L. Hirshfield, M. A. LaPointe, O. A. Nezhevenko, S. H. Gold, and A. K. Kinkead, "Active compression of RF pulses," *Quasi-optical Control of Intense Microwave Transmission*, J. L. Hirshfield and M. I. Petelin (eds.), 199–218, Springer, Netherlands, 2005.
3. Yushkov, Y. G., N. N. Badulin, A. P. Batsula, A. I. Mel'nikov, S. A. Novikov, S. V. Razin, and E. L. Shoshin, "A nanosecond pulse-compression microwave radar," *Telecommunications and Radio Engineering*, Vol. 54, No. 2, 92–98, 2000.

4. Schamiloglu, E., "High power microwave sources and applications," *2004 IEEE MTT-S Digest*, 1001–1004, 2004.
5. Benford, J., "Space applications of high-power microwaves," *IEEE Trans. Plasma Sci.*, Vol. 36, No. 3, 569–581, 2008.
6. Gaponov-Grekhov, A. V. and V. L. Granatstein, *Applications of High-power Microwaves*, Artech House, Boston, 1994.
7. Bluhm, H., *Pulsed Power Systems. Principles and Applications*, Springer, Berlin, 2006.
8. Andreev, A. D., E. G. Farr, and E. Schamiloglu, "A simplified theory of microwave pulse compression," *Circuit and Electromagnetic System Design Notes*, No. 57, 2008.
9. Baum, C. E., "Options in microwave pulse compression," *Circuit and Electromagnetic System Design Notes*, No. 68, 2010.
10. Vikharev, A. L., A. M. Gorbachev, O. A. Ivanov, V. A. Isaev, S. V. Kuzikov, B. Z. Movshevich, J. L. Hirshfield, and S. H. Gold, "Active Bragg compressor of 3-cm wavelength microwave pulses," *Radiophys. Quantum Electron.*, Vol. 51, No. 7, 539–555, 2008.
11. Artemenko, S. N., V. A. Avgustinovich, V. L. Kaminskii, P. Y. Chumerin, and Y. G. Yushkov, "Experimental investigation of a 25-MW microwave (3-cm range) compressor prototype," *Technical Physics*, Vol. 45, No. 12, 1608–1611, 2000.
12. Tantawi, S. G., R. D. Ruth, A. E. Vlieks, and M. Zolotarev, "Active high-power RF pulse compression using optically switched resonant delay lines," *IEEE Trans. Microw. Theory Tech.*, Vol. 45, No. 8, 1486–1492, 1997.
13. Vikharev, A. L., A. M. Gorbachev, O. A. Ivanov, V. A. Isaev, S. V. Kuzikov, A. L. Kolysko, and M. I. Petelin, "Active microwave pulse compressor utilizing an axisymmetric mode of a circular waveguide," *Technical Physics Letters*, Vol. 24, No. 10, 791–792, 1998.
14. Farr, E. G., L. H. Bowen, W. D. Prather, and C. E. Baum, "Microwave pulse compression experiments at low and high power," *Circuit and Electromagnetic System Design Notes*, No. 63, 2010.
15. Tamura, F. and S. G. Tantawi, "Development of high power X-band semiconductor microwave switch for pulse compression systems of future linear colliders," *Phys. Rev. Spec. Top. Accel. Beams*, Vol. 5, 062001, 2002.
16. Ivanov, O. A., A. A. Vikharev, A. M. Gorbachev, V. A. Isaev, M. A. Lobaev, A. L. Vikharev, S. V. Kuzikov, J. L. Hirshfield, and M. A. LaPointe, "Active quasi-optical Ka-band rf pulse compressor

- switched by a diffraction grating," *Phys. Rev. Spec. Top. Accel. Beams*, Vol. 12, 093501, 2009.
17. Kuzmitchev, I. K., P. M. Melezhyk, V. L. Pazynin, K. Y. Sirenko, Y. K. Sirenko, O. S. Shafalyuk, and L. G. Velychko, "Model synthesis of energy compressors," *Radiophysics and Electronics: Sci. Works Collection*, Vol. 13, No. 2, 166–172, 2008.
 18. Chernobrovkin, R. E., I. V. Ivanchenko, A. M. Korolev, N. A. Popenko, and K. Y. Sirenko, "The novel microwave stop-band filter," *Active and Passive Electronic Components*, Vol. 2008, 2008.
 19. Sirenko, K., V. Pazynin, Y. Sirenko, and H. Bagci, "An FFT-accelerated FDTD scheme with exact absorbing conditions for characterizing axially symmetric resonant structures," *Progress In Electromagnetics Research*, Vol. 111, 331–364, 2011.
 20. Sirenko, K. Y. and Y. K. Sirenko, "Exact absorbing conditions in the initial boundary-value problems of the theory of open waveguide resonators," *Comput. Math. Math. Phys.*, Vol. 45, No. 3, 490–506, 2005.
 21. Sirenko, Y. K., S. Strom, and N. P. Yashina, *Modeling and Analysis of Transient Processes in Open Resonant Structures. New Methods and Techniques*, Springer, Berlin, 2007.
 22. Hairer, E., C. H. Lubich, and M. Schlichte, "Fast numerical solution of nonlinear Volterra convolution equations," *SIAM J. Sci. Stat. Comput.*, Vol. 6, No. 3, 532–541, 1985.
 23. Yilmaz, A. E., D. S. Weile, B. Shanker, J.-M. Jin, and E. Michielssen, "Fast analysis of transient scattering in lossy media," *IEEE Antennas Wireless Propagat. Lett.*, Vol. 1, No. 1, 14–17, 2002.
 24. Bagci, H., A. E. Yilmaz, and E. Michielssen, "A fast hybrid TDIE-FDTD-MNA scheme for analyzing cable-induced transient coupling into shielding enclosures," *Proc. IEEE Int. Symp. Electromagn. Compat.*, Vol. 3, 828–833, 2005.
 25. Bagci, H., A. E. Yilmaz, V. Lomakin, and E. Michielssen, "Fast solution of mixed-potential time-domain integral equations for half-space environments," *IEEE Trans. Geosci. Remote Sensing*, Vol. 43, No. 2, 269–279, 2005.
 26. Bagci, H., A. E. Yilmaz, and E. Michielssen, "FFT-accelerated MOT-based solution of time-domain BLT equations," *Proc. IEEE Int. Antennas Propagat. Symp.*, 1175–1178, 2006.
 27. Bagci, H., A. E. Yilmaz, J.-M. Jin, and E. Michielssen, "Fast and rigorous analysis of EMC/EMI phenomena on electrically large

- and complex structures loaded with coaxial cables,” *IEEE Trans. Electromagn. Compat.*, Vol. 49, No. 2, 361–381, 2007.
28. Bagci, H., A. E. Yilmaz, and E. Michielssen, “An FFT-accelerated time-domain multiconductor transmission line simulator,” *IEEE Trans. Electromagn. Compat.*, Vol. 52, No. 1, 199–214, 2010.
 29. Sirenko, Y. K., L. G. Velychko, and F. Erden, “Time-domain and frequency-domain methods combined in the study of open resonance structures of complex geometry,” *Progress In Electromagnetics Research*, Vol. 44, 57–79, 2004.
 30. Velychko, L. G., Y. K. Sirenko, and O. S. Shafalyuk, “Time-domain analysis of open resonators. Analytical grounds,” *Progress In Electromagnetics Research*, Vol. 61, 1–26, 2006.
 31. Velychko, L. G. and Y. K. Sirenko, “Controlled changes in spectra of open quasi-optical resonators,” *Progress In Electromagnetics Research B*, Vol. 16, 85–105, 2009.
 32. Karmel, P. R., G. D. Colef, and R. L. Camisa, *Introduction to Electromagnetic and Microwave Engineering*, John Wiley, New York, 1998.
 33. Shestopalov, V. P., A. A. Kirilenko, and L. A. Rud’, *Resonance Wave Scattering. Vol. 2. Waveguide Discontinuities*, Naukova Dumka, Kiev, 1986 (in Russian).
 34. Pozar, D. M., *Microwave Engineering*, Wiley, New York, 1998.
 35. Belous, O. I., A. A. Kirilenko, V. I. Tkachenko, A. I. Fisun, and A. M. Fursov, “Excitation of an open stripline resonator by a plane waveguide,” *Radiophys. Quantum Electron.*, Vol. 37, No. 3, 181–189, 1994.
 36. Sirenko, Y. K. and S. Strom, *Modern Theory of Gratings. Resonant Scattering: Analysis Techniques and Phenomena*, Springer, Berlin, 2010.
 37. Taflove, A. and S. C. Hagness, *Computational Electrodynamics: The Finite-difference Time-domain Method*, Artech House, Boston, 2005.